THE JOURNAL OF PHYSICAL CHEMISTRY C

Article

pubs.acs.org/JPCC

Atomic Layer Etching of AlF_3 Using Sequential, Self-Limiting Thermal Reactions with $Sn(acac)_2$ and Hydrogen Fluoride

Younghee Lee,[†] Jaime W. DuMont,[†] and Steven M. George*[,†,‡]

[†]Department of Chemistry and Biochemistry and [‡]Department of Mechanical Engineering, University of Colorado at Boulder, Boulder, Colorado 80309, United States

ABSTRACT: The atomic layer etching (ALE) of AlF_3 was demonstrated using sequential thermal reactions with $Sn(acac)_2$ and hydrogen fluoride (HF) as the reactants. AlF_3 ALE is the first example of the thermal ALE of a metal fluoride. AlF_3 ALE was investigated using in situ quartz crystal microbalance (QCM) and Fourier transform infrared (FTIR) measurements at temperatures from 150 to 250 °C. The QCM studies observed that AlF_3 was etched linearly with atomic level precision versus number of sequential reactant cycles. QCM investigations also revealed that the sequential $Sn(acac)_2$ and HF reactions were self-limiting versus reactant exposure. The FTIR spectroscopic analysis observed AlF_3 etching by monitoring the loss of absorbance of Al−F stretching vibrations in the AlF_3 film. The FTIR studies also suggested that the $Sn(acac)_2$ reaction is self-limiting because of the buildup of acac-containing species on the AlF_3 surface. The QCM measurements determined that the mass change per cycle (MCPC) increased with temperature from −2.0 ng/(cm^2 cycle) at 150 °C to −18.2 ng/(cm^2 cycle) at 250 °C. These MCPC values are equivalent to etch rates from 0.069 Å/cycle at 150 °C to 0.63 Å/cycle at 250 °C. In the proposed reaction mechanism for AlF_3 ALE, the $Sn(acac)_2$ reactant accepts fluorine from AlF_3 and donates acac to the surface. This reaction is believed to yield SnF(acac) and $AlF(acac)_2$ as volatile reaction products. The QCM and FTIR results suggest that the HF reaction converts $AlF_2(acac)$* surface intermediates to AlF_3* and volatile acacH reaction products. The ALE of other metal fluorides using $Sn(acac)_2$ and HF should be possible by a similar mechanism.

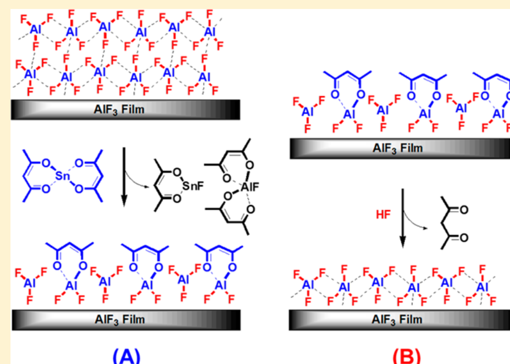

I. INTRODUCTION

Atomic layer etching (ALE) is a thin film removal process based on sequential, self-limiting surface reactions.[1−3] ALE can be viewed as the reverse of atomic layer deposition (ALD).[3−5] Most previous ALE processes have used halogenation of the surface together with ion-enhanced or energetic neutral atom beam-enhanced surface reactions to etch the material. This ALE approach can achieve anisotropic etching and has been used for the ALE of Si,[6−9] Ge,[10] compounds semiconductors,[11−14] metal oxides,[15−18] and various carbon substrates.[19−21] In contrast to the large number of ALE processes accomplished using ion-enhanced or energetic neutral atom beams, there are very few ALE processes based on spontaneous thermal chemistry. These thermal ALE processes could be valuable for the conformal and isotropic removal of thin films with atomic layer control.[2]

Recently, thermal ALE has been reported for two metal oxides. Al_2O_3 ALE[22,23] and HfO_2 ALE[24] were demonstrated using sequential, self-limiting thermal reactions with $Sn(acac)_2$ and hydrogen fluoride (HF) as the reactants. The overall Al_2O_3 ALE reaction was believed to be $Al_2O_3 + 6Sn(acac)_2 + 6HF \rightarrow 2Al(acac)_3 + 6SnF(acac) + 3H_2O$.[22,23] The overall HfO_2 ALE reaction was suggested to be $HfO_2 + 4Sn(acac)_2 + 4HF \rightarrow Hf(acac)_4 + 4SnF(acac) + 2H_2O$.[24] For Al_2O_3 and HfO_2 ALE, metal fluorides in the form of AlF_3* and HfF_4*, respectively, were the proposed surface reaction intermediates after the HF exposures.[22−24] The asterisks designate the surface species. In the proposed reaction mechanism, the metal fluorides donate fluorine to $Sn(acac)_2$ to form a volatile SnF(acac) reaction product. Concurrently, $Sn(acac)_2$ releases acac ligand to the metal in the metal fluoride to form volatile metal acac reaction products.[22−24] This ligand-exchange process is a type of transmetalation reaction.[25]

Because AlF_3* plays a key role as a surface reaction intermediate during Al_2O_3 ALE,[22] AlF_3 ALE may also be possible using the same reactants. In this study, the thermal ALE of AlF_3 was performed using $Sn(acac)_2$ and HF as the reactants. Based on the previous mechanism for Al_2O_3 ALE,[22,23] the fluorination reaction during AlF_3 ALE may not be expected to be needed because AlF_3 is already the starting material. However, the experiments reveal that the HF reactant is necessary for AlF_3 ALE. The $Sn(acac)_2$ reactant is believed to accept fluorine from the AlF_3 to form a volatile SnF(acac) reaction product. The acac ligands donated to the AlF_3 surface from $Sn(acac)_2$ also lead to the removal of volatile acac-containing aluminum species. In addition, the donated acac ligands produce $AlF_2(acac)$ and other acac-containing surface species that are thought to limit the $Sn(acac)_2$ etching reaction.

Received: July 26, 2015
Revised: October 16, 2015
Published: October 19, 2015

ACS Publications © 2015 American Chemical Society

DOI: 10.1021/acs.jpcc.5b07236
J. Phys. Chem. C 2015, 119, 25385−25393

The HF reactant then facilitates the removal or conversion of the acac-containing species on the AlF_3 surface.

In this paper, thermal AlF_3 ALE is demonstrated using in situ quartz crystal microbalance (QCM) and Fourier transform infrared (FTIR) experiments. QCM analysis is used to study the etching of AlF_3 versus the number of $Sn(acac)_2$ and HF reaction cycles. The self-limiting behavior of AlF_3 ALE is explored versus the $Sn(acac)_2$ and HF exposure times. In addition, the temperature dependence of AlF_3 ALE is examined from 150 to 250 °C. FTIR vibrational spectroscopy analysis is also able to monitor the AlF_3 etching and characterize the surface species after the $Sn(acac)_2$ and HF exposures. These results for AlF_3 ALE expand the possibilities for thermal ALE reactions beyond metal oxides to metal fluorides.

II. EXPERIMENTAL SECTION

A. Viscous Flow Reactor Equipped for in Situ QCM Measurements. The ALE reactions were conducted in a viscous flow ALD reactor.[22−24] The reaction temperatures varied from 150 to 250 °C. A proportional-integral-derivative (PID) temperature controller (2604, Eurotherm) held the temperature constant to within ±0.04 °C. The reactor pressure was measured using a capacitance manometer (Baratron 121A, MKS).

The ALD reactor was outfitted with an in situ QCM.[22−24] An RC-cut quartz crystal (gold coated and polished, 6 MHz, Colnatec) was positioned in a sensor head (BSH-150, Inficon). The sensor head was then sealed with a high-temperature epoxy (Epo-Tek H21D, Epoxy technology). A thin film deposition monitor (Maxtek TM-400, Inficon) was employed to record the QCM measurements.

Sequential exposures of tin(II) acetylacetonate ($Sn(acac)_2$, 37−38% Sn, Gelest) and HF-pyridine (70 wt % HF, Sigma-Aldrich) were employed for the AlF_3 ALE reactions. Gaseous HF from HF-pyridine is a much safer source of anhydrous HF than HF from a gas cylinder. HF-pyridine exists as a liquid at room temperature and is in equilibrium with gaseous HF. At room temperature, the HF pressure above HF-pyridine is 90−100 Torr.[24]

HF-pyridine and $Sn(acac)_2$ were both transferred to stainless steel bubblers using a dry N_2-filled glovebag.[22−24] The $Sn(acac)_2$ precursor was held at 100 °C and produced a pressure transient of 20 mTorr during $Sn(acac)_2$ exposures. The HF-pyridine precursor was maintained at room temperature and produced a pressure transient of 80 mTorr during HF exposures. The AlF_3 films were grown by AlF_3 ALD using TMA (97%, Sigma-Aldrich) and HF derived from HF-pyridine.[26] The TMA precursor was held at room temperature.

A mechanical pump (Pascal 2015SD, Alcatel) was employed to pump the reactor. A constant total flow of 150 sccm of ultrahigh-purity (UHP) N_2 carrier gas into the reactor was delivered by three separate mass flow controllers (Type 1179A, MKS). Additional N_2 gas flow of 20 sccm was provided using a metering bellows-sealed valve (SS-4BMG, Swagelok) to prevent deposition on the backside of the QCM crystal.[27] A base pressure of ∼1 Torr in the reactor was produced by the total N_2 gas flow of 170 sccm.

B. Reactor for in Situ FTIR Spectroscopy Measurements. The in situ FTIR studies were conducted in a reactor interfaced to an FTIR spectrometer.[22,24,28] The reactor was pumped with a mechanical pump (TRIVAC D8B, Oerlikon Leybold Vacuum). The FTIR spectrometer (Nicolet 6700 FTIR, Thermo Scientific) was equipped with a liquid-N_2-cooled mercury cadmium telluride (MCT-B) detector. The spectrometer, mirror, and detector setup were purged using dry, CO_2-free air. A total of 100 scans at 4 cm^{-1} resolution were recorded for each spectrum from 400 to 4000 cm^{-1}.

The transmission FTIR measurements were conducted using high surface area SiO_2 nanoparticles (99.5%, U.S. Research Nanomaterials). These SiO_2 nanoparticles had an average diameter of 15−20 nm. The high surface area of the SiO_2 nanoparticles enhanced the concentration of surface species in the infrared beam.[29,30] The SiO_2 nanoparticles absorb in the infrared region between 400−650 cm^{-1}, 700−875 cm^{-1}, and 925−1400 cm^{-1}. These absorptions leave open windows to monitor absorbance from the AlF_3 ALD film.[26] Samples were prepared by pressing the SiO_2 nanoparticles into a tungsten grid support (Tech-Etch). The dimensions of tungsten grids were 2 cm × 3 cm. The thickness of the grid was 50 μm thick, and the grid had 100 lines per inch.

A dc power supply (6268B, 20 V/20A, Hewlett-Packard) was used to resistively heat the tungsten grid. A PID temperature controller (Love Controls 16B, Dwyer Instruments) defined the voltage output of the power supply. A type K thermocouple was fixed to the bottom of the tungsten grid with epoxy (Ceramabond 571, Aremco). The epoxy also electrically isolated the thermocouple from the tungsten grid.

The AlF_3 films were grown with AlF_3 ALD using TMA (97%, Sigma-Aldrich) and HF from HF-pyridine (70 wt % HF, Sigma-Aldrich) at 150 °C.[26] The AlF_3 ALE reactions were conducted using sequential exposures of tin(II) acetylacetonate ($Sn(acac)_2$, 37−38% Sn, Gelest) and HF from HF-pyridine at 250 °C. Self-limiting reactions were obtained using two consecutive $Sn(acac)_2$ doses with exposure times of 2.0 s and two consecutive HF doses with exposure times of 2.0 s. Pressure transients for $Sn(acac)_2$ and HF of ∼350 and ∼400 mTorr, respectively, above the base pressure were observed using these exposure times. A 180 s purge time was employed after each reactant exposure.

Reactants were dosed into a flowing N_2 carrier gas stream. The constant N_2 carrier gas flow rate of 50 sccm was supplied by a mass flow controller. This N_2 gas flow produced a base pressure of ∼0.650 Torr in the reactor. The TMA, HF-pyridine, and H_2O precursors were maintained at room temperature. The $Sn(acac)_2$ precursor was held at 100 °C.

III. RESULTS AND DISCUSSION

A. Quartz Crystal Microbalance (QCM) Studies. Figure 1 shows the mass change during 100 ALE cycles of sequential $Sn(acac)_2$ and HF reactions on an AlF_3 film at 200 °C. One ALE cycle was defined by a $Sn(acac)_2$ dose of 1 s, a N_2 purge of 30 s, a HF dose of 1.0 s, and a second N_2 purge of 30 s. This reaction sequence is denoted as 1−30−1−30. The initial AlF_3 film on the QCM surface was grown by 100 cycles of AlF_3 ALD using TMA and HF.[26]

The etching of the AlF_3 film is very linear and displays a mass change per cycle (MCPC) = −6.1 ng/(cm^2 cycle) at 200 °C. This MCPC corresponds to an etch rate of 0.21 Å/cycle at 200 °C based on the AlF_3 ALD film density of 2.9 g/cm^3 that was measured by X-ray reflectivity (XRR).[26] All ALE cycles show mass losses due to etching of the AlF_3 film except for the first cycle.

Figure 2 displays a magnification of the mass changes during the first three AlF_3 ALE cycles at 200 °C in Figure 1. The first AlF_3 ALE cycle shows a mass gain of ΔM_{Sn} = 28 ng/cm^2 and a mass loss of ΔM_{HF} = −8 ng/cm^2. The subsequent AlF_3 ALE

DOI: 10.1021/acs.jpcc.5b07236
J. Phys. Chem. C 2015, 119, 25385−25393

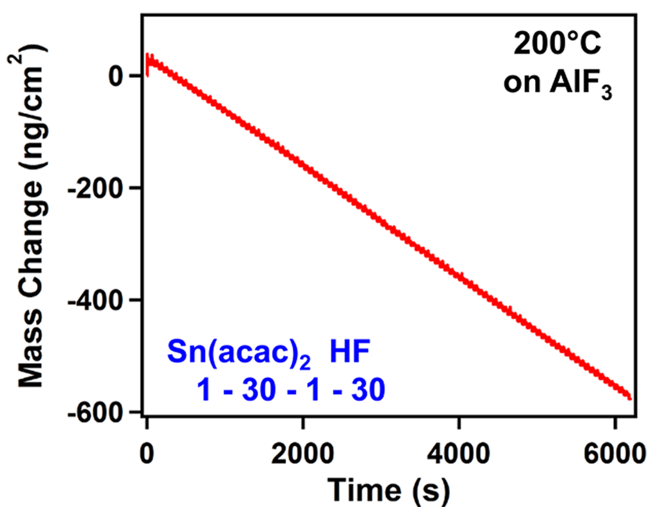

Figure 1. Mass change versus time for AlF_3 ALE using sequential $Sn(acac)_2$ and HF exposures at 200 °C.

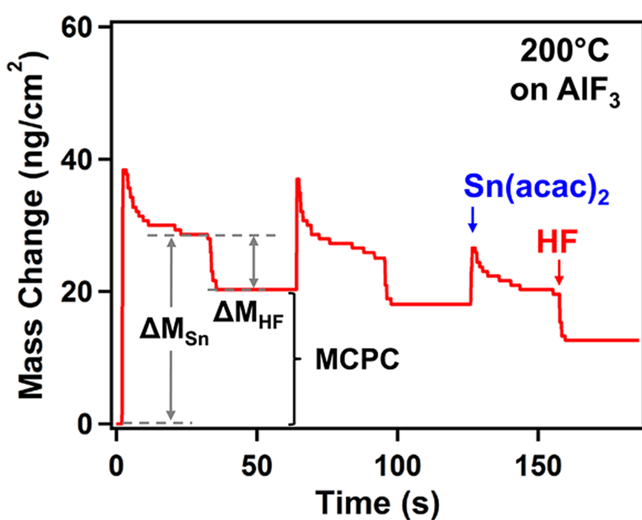

Figure 2. Expansion of the first three cycles in Figure 1 showing the mass changes during the $Sn(acac)_2$ and HF exposures at 200 °C.

cycles then produce overall mass losses as illustrated in Figures 1 and 2. The mass gain for ΔM_{Sn} on the first cycle is assigned to the adsorption of $Sn(acac)_2$ reaction products on the AlF_3 surface. The $Sn(acac)_2$ could either adsorb associatively as $Sn(acac)_2$* or dissociatively as Sn(acac)* and (acac)*. The $Sn(acac)_2$ could also react to form AlF_2(acac)* surface intermediates.

To estimate the coverage of acac-containing species on the AlF_3 surface, the sites on the AlF_3 surface can be approximated using the density of 2.9 g/cm^3 for AlF_3 ALD films.[26] This mass density is equivalent to a number density of $\rho = 2.08 \times 10^{22}$ (AlF_3 units)/cm^3. This number density yields an estimate for the number of AlF_3 units on the AlF_3 surface of $\rho^{2/3} = 7.56 \times 10^{14}$ (AlF_3 units)/cm^2 assuming a square lattice. This coverage of AlF_3 units represents an AlF_3 mass of 105.5 ng/cm^2.

The coverage of acac-containing species can then be estimated based on the mass gain of 28 ng/cm^2 and assuming that $Sn(acac)_2$ does not form volatile etch products during the first cycle. This mass gain is equivalent to 5.32×10^{13} $Sn(acac)_2$/cm^2. This coverage of $Sn(acac)_2$ is about one-half the $Sn(acac)_2$* coverage of 1.16×10^{14} $Sn(acac)_2$/cm^2 measured on Al_2O_3 during the first $Sn(acac)_2$ exposure during Al_2O_3 ALE.[22] The normalized coverage of $Sn(acac)_2$* species relative to AlF_3 units on the surface is (5.32×10^{13} $Sn(acac)_2$/cm^2)/(7.56×10^{14} (AlF_3 units)/cm^2) = 0.07 $Sn(acac)_2$/(AlF_3 unit).

The relatively low coverage of $Sn(acac)_2$* or other acac-containing species may be explained by the bulky acetylacetonate ligand that is expected to occupy more than one AlF_3 unit on the AlF_3 surface. In comparison, the $Sn(acac)_2$* coverage on Al_2O_3 after the first $Sn(acac)_2$ exposure during Al_2O_3 ALE was 0.17 $Sn(acac)_2$/(Al_2O_3 unit).[22] Another explanation for the low coverage is that there is etching during the first $Sn(acac)_2$ exposure on AlF_3 that releases volatile reaction products and decreases the mass gain. The lower mass gain would decrease the coverage calculated for the acac-containing species from the first $Sn(acac)_2$ exposure.

Figure 2 also displays distinct mass losses that coincide with HF exposures during AlF_3 ALE. These mass losses are explained by the removal of acac-containing species from the AlF_3 surface remaining after the $Sn(acac)_2$ exposure. Acac-containing surface species such as AlF_2(acac)* could be fluorinated by HF to produce AlF_3* and volatile acacH reaction product. Other acac-containing species such as acac* could also be protonated to produce a volatile acacH reaction product. The boiling point of acetylacetone (acacH) is 138 °C at 760 Torr.[31] In comparison, mass gains are observed during HF exposures in Al_2O_3 ALE.[22,23] A mass gain is observed during HF exposures in Al_2O_3 ALE because of the conversion of Al_2O_3 to AlF_3.[22,23] A mass gain during HF exposures in AlF_3 ALE is not expected because AlF_3 is already a stable fluoride.

Figure 2 also reveals mass gains at 200 °C during the $Sn(acac)_2$ exposures after the first cycle. These mass gains may be surprising because they occur during the removal of fluorine and aluminum from the surface by ligand-exchange reactions. Fluorine can be donated to $Sn(acac)_2$ to produce volatile SnF(acac) reaction products. $Sn(acac)_2$ has a vapor pressure of 0.5 Torr at 102−105 °C.[32] There are no reports for the vapor pressure of SnF(acac). However, the analogous compound SnCl(acac) is known to sublime at 100−115 °C at 0.5 Torr.[32] The acac ligands donated to the AlF_3 surface can also lead to the production of volatile $Al(acac)_3$ or $AlF(acac)_2$ reaction products. $Al(acac)_3$ has a vapor pressure of ~3−4 Torr at 150 °C.[33,34] There are no reports for the vapor pressure of $AlF(acac)_2$.

The mass gains at 200 °C that coincide with $Sn(acac)_2$ exposures during AlF_3 ALE indicate that there are mass additions during the $Sn(acac)_2$ exposures that offset the mass losses resulting from the removal of fluorine and aluminum. Possible mass additions are the massive acac groups in adsorbed species such as AlF_2(acac)* or $AlF(acac)_2$* on the AlF_3 surface after the ligand-exchange reaction. The addition of these acac-containing adsorbed species after the $Sn(acac)_2$ exposures then leads to mass losses that are observed during the HF exposures.

The exact reactions that explain the mass losses during the HF exposure and mass gains during the $Sn(acac)_2$ exposures at 200 °C are not known. One of the biggest unknowns is the gas phase reaction products. These reaction products have not yet been confirmed using quadrupole mass spectrometry. These measurements require mass spectrometers that can detect signals at higher masses than are typical for mass spectrometers used for residual gas analysis. These studies will be a goal of future investigations.

DOI: 10.1021/acs.jpcc.5b07236
J. Phys. Chem. C 2015, 119, 25385−25393

Figure 3 shows a magnification of the mass changes versus time for three cycles at 200 °C in the linear loss regime shown

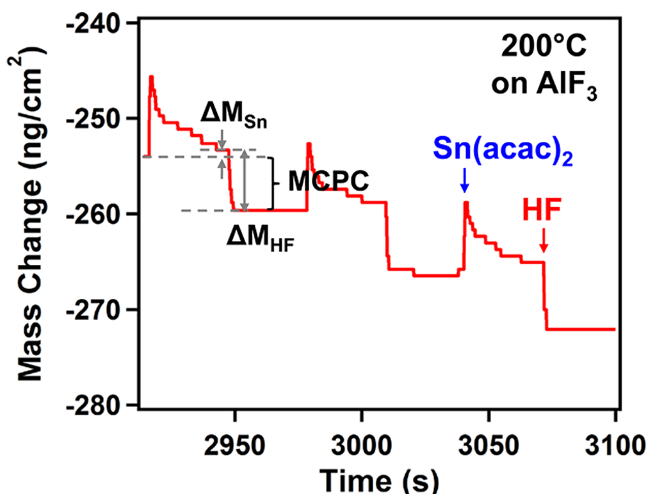

Figure 3. Expansion of the linear loss regime in Figure 1 showing the mass changes during three cycles of $Sn(acac)_2$ and HF exposures at 200 °C.

in Figure 1. In agreement with the results in Figure 2, mass gains are observed during the $Sn(acac)_2$ exposures and mass losses are observed during the HF exposures. A progressive mass loss after the $Sn(acac)_2$ exposures suggests that the acac-containing species have a mild interaction with the AlF_3 surface and may slowly desorb versus time. Following the $Sn(acac)_2$ adsorption and proposed desorption of reaction products, Figure 3 shows that a mass gain of ΔM_{Sn} = 0.8 ng/cm² is observed prior to the HF exposure. The HF exposure then leads to a sharp mass decrease of ΔM_{HF} = −6.9 ng/cm² that may be consistent with the conversion of $AlF_2(acac)$* surface intermediates to AlF_3* and volatile acacH.

Figure 4 shows the MCPC and the ΔM_{Sn}/MCPC ratio during 100 cycles of AlF_3 ALE at 200 °C. The MCPC is defined by MCPC = ΔM_{Sn} + ΔM_{HF}. Figure 4a displays ΔM_{Sn}, ΔM_{HF}, and MCPC for the same 100 cycles of AlF_3 ALE at 200 °C as shown in Figure 1. The MCPC reaches a steady-state value of −6.1 ng/(cm² cycle) after a nucleation period of five cycles. Figure 4b displays the ΔM_{Sn}/MCPC ratio during the same 100 cycles. The ΔM_{Sn}/MCPC ratio reaches a steady-state value of −0.13 after five cycles of nucleation. The ΔM_{Sn}/MCPC ratio will be employed to define the stoichiometry of the AlF_3 ALE reactions.

Figure 5 reveals the self-limiting nature of the AlF_3 ALE reactions at 200 °C studied by measuring the MCPC for different reactant exposures. Figure 5a examines the self-limiting behavior of the $Sn(acac)_2$ reaction using different $Sn(acac)_2$ exposure times with a single 1.0 s dose of HF. A constant N_2 purge of 30 s was used after each exposure. This reaction sequence can be denoted as x−30−1−30. The MCPC versus $Sn(acac)_2$ exposure time decreases and levels off at a MCPC of approximately −6 ng/(cm² cycle). The solid line is an exponential fit to the data that is intended to guide the eye. The approximately self-limiting behavior for $Sn(acac)_2$ is somewhat unexpected because the continuous etching of AlF_3 by $Sn(acac)_2$ could occur if the SnF(acac), $AlF(acac)_2$, or $Al(acac)_3$ reaction products can desorb from the surface. The self-limiting behavior suggests that acac-containing surface species must remain on the AlF_3 surface and impede the etching reaction.

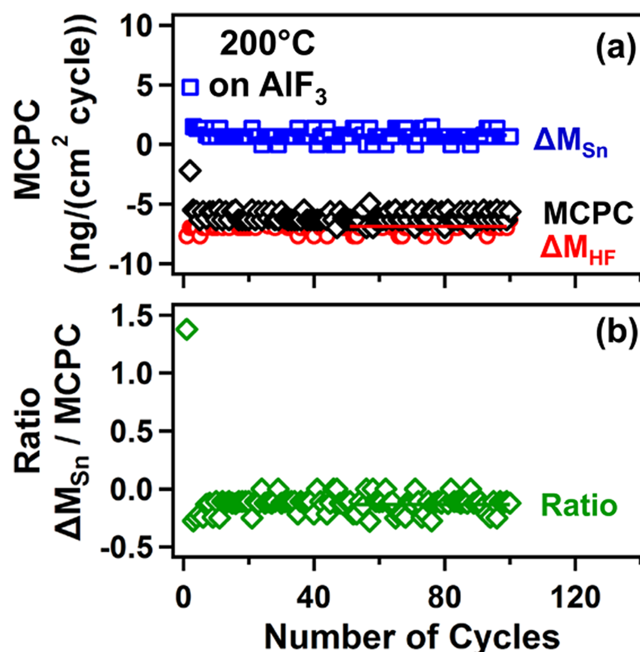

Figure 4. (a) Mass change after the $Sn(acac)_2$ exposure (ΔM_{Sn}), mass change after the HF exposure (ΔM_{HF}), and mass change per cycle (MCPC) versus number of ALE cycles at 200 °C. (b) ΔM_{Sn}/MCPC ratio versus number of ALE cycles.

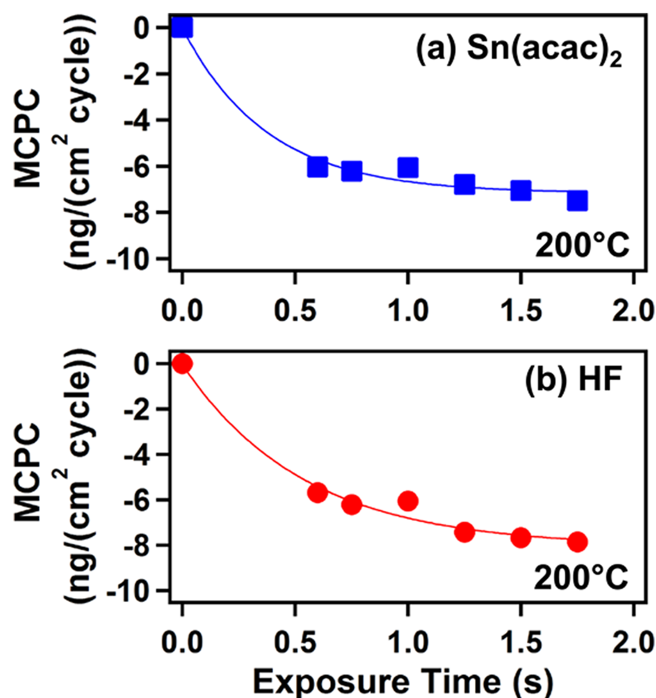

Figure 5. Mass change per cycle (MCPC) for AlF_3 ALE versus exposure time at 200 °C for (a) $Sn(acac)_2$ and (b) HF.

Figure 5b examines the self-limiting behavior of the HF reaction using different HF exposure times with a single 1.0 s dose of $Sn(acac)_2$. This reaction sequence can be denoted as 1−30−x−30. The MCPC versus HF exposure time decreases and levels off at a MCPC of approximately −6 ng/(cm² cycle). The solid line is again an exponential fit to the data that is

DOI: 10.1021/acs.jpcc.5b07236
J. Phys. Chem. C 2015, 119, 25385−25393

included to guide the eye. A slight increase in the MCPC is also observed at longer HF exposures. This additional mass loss is attributed to chemical vapor etching (CVE) resulting from HF partial pressure in the reactor during the $Sn(acac)_2$ exposures.[24] CVE will occur if both HF and $Sn(acac)_2$ are present in the reactor at the same time. CVE may result at the larger HF exposures because of the difficulty removing all the HF prior to the $Sn(acac)_2$ exposure.

Figure 6 shows the mass changes during three ALE cycles in the linear loss regime of $Sn(acac)_2$ and HF reactions on an AlF_3 surface at a lower temperature of 150 °C using a reaction sequence of 1−30−1−30. The initial AlF_3 film was again prepared by 100 cycles of AlF_3 ALD using TMA and HF.[26] The etching of the AlF_3 film is linear and displays a MCPC of −2.0 ng/(cm^2 cycle). This MCPC corresponds to an etch rate of 0.069 Å/cycle based on the AlF_3 ALD film density of 2.9 g/cm^3 measured by XRR.[26]

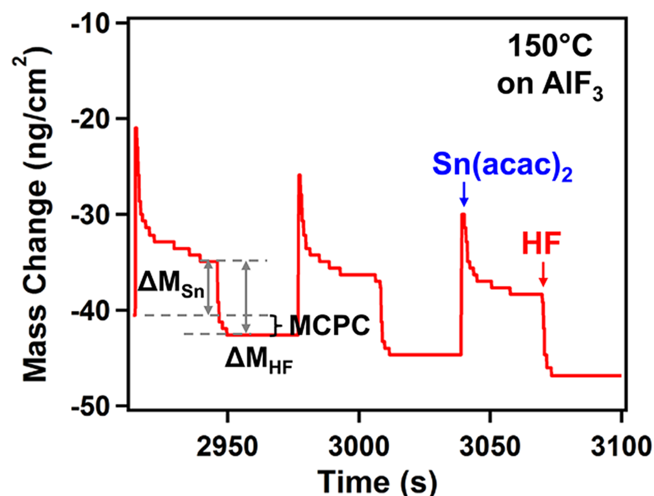

Figure 6. Individual mass changes during three cycles of sequential $Sn(acac)_2$ and HF exposures in the linear loss regime for AlF_3 ALE at 150 °C.

There is a distinct difference between the mass changes during the AlF_3 ALE reactions at 200 and 150 °C. A mass gain of ΔM_{Sn} = 5.5 ng/cm^2 was observed after 1.0 s of $Sn(acac)_2$ exposure at 150 °C. In comparison, a smaller mass gain of ΔM_{Sn} = 0.8 ng/cm^2 was obtained at 200 °C. This difference may be attributed to less etching and possibly more adsorption of acac-containing species on the AlF_3 surface at lower temperatures. The mass decrease of ΔM_{HF} = −7.5 ng/cm^2 observed after the HF exposures at 150 °C is similar to the mass decrease of ΔM_{HF} = −6.9 ng/cm^2 observed after the HF exposures at 200 °C.

Figure 7 shows the mass changes during three ALE cycles of $Sn(acac)_2$ and HF reactions on an AlF_3 surface at a higher temperature of 250 °C. These results were also recorded in the linear loss regime using a reaction sequence of 1−30−1−30 after depositing the initial AlF_3 film using 100 cycles of AlF_3 ALD.[26] The etching of the AlF_3 film is linear and displays a MCPC of −18.2 ng/(cm^2 cycle). This MCPC corresponds to an etch rate of 0.63 Å/cycle.

The mass changes in Figure 7 at 250 °C are very different than the mass changes during the AlF_3 ALE reactions at 150 and 200 °C. At the higher temperature of 250 °C, a mass loss of ΔM_{Sn} = −12.0 ng/cm^2 is observed after the $Sn(acac)_2$ exposures. In comparison, mass gains after the $Sn(acac)_2$

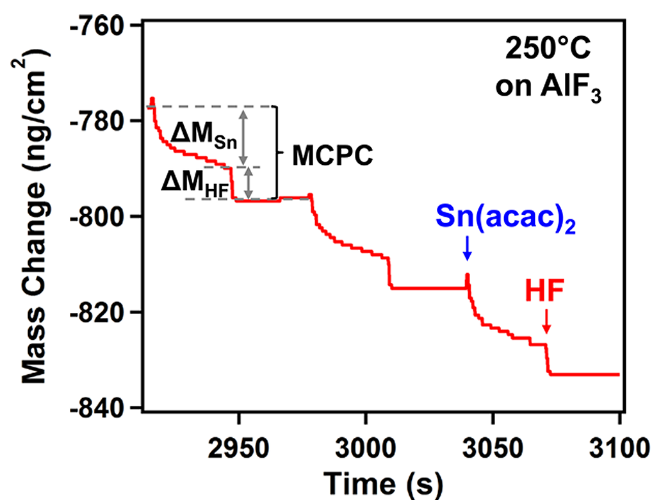

Figure 7. Individual mass changes during three cycles of sequential $Sn(acac)_2$ and HF exposures in the linear loss regime for AlF_3 ALE at 250 °C.

exposures of ΔM_{Sn} = 5.5 ng/cm^2 and 0.8 ng/cm^2 were obtained at 150 and 200 °C, respectively. The mass loss for ΔM_{Sn} at 250 °C is attributed to more etching and possibly less adsorption of acac-containing species on the AlF_3 surface at higher temperatures.

Similar to the behavior observed in Figures 2, 3, and 6, Figure 7 also shows a progressive mass loss after the $Sn(acac)_2$ exposures. This mass loss suggests that the acac-containing species slowly desorb from the AlF_3 surface versus time. Figure 7 also observes a mass decrease of ΔM_{HF} = −6.2 ng/cm^2 after the HF exposures at 250 °C. This mass decrease is similar to the mass decreases observed after the HF exposures at 150 and 200 °C. The dependences of ΔM_{Sn}, ΔM_{HF}, and MCPC on the reaction temperature are all summarized in Table 1.

Table 1. ΔM_{Sn}, ΔM_{HF}, MCPC, ΔM_{Sn}/MCPC, y, and y(MCPC) for AlF_3 ALE at Different Temperatures[a]

temp (°C)	MCPC	ΔM_{Sn}	ΔM_{HF}	ΔM_{Sn}/MCPC	y	y(MCPC)
150	−2.0	5.5	−7.5	−2.8	4.0	−7.9
200	−6.1	0.8	−6.9	−0.13	1.2	−7.2
250	−18.2	−12.0	−6.2	0.66	0.4	−6.5

[a] ΔM_{Sn}, ΔM_{HF}, MCPC, and y(MCPC) are expressed in units of ng/(cm^2 cycle).

B. Fourier Transform Infrared (FTIR) Studies. Figure 8 shows the growth of absorbance from 500 to 900 cm^{-1} after various numbers of AlF_3 ALD cycles on SiO_2 nanoparticles at 150 °C. Similar results were reported earlier during the study of AlF_3 ALD.[26] These FTIR spectra were referenced to the FTIR spectrum for the initial SiO_2 nanoparticles. The absorbance increased progressively versus number of AlF_3 ALD cycles. The growth of absorbance from 500 to 900 cm^{-1} is assigned to the Al−F stretching vibrations in AlF_3.[26] Previous vibrational studies have monitored the absorption of Al−F stretching vibrations in AlF_3 at 500−900 cm^{-1}.[35−38]

Figure 8 also displays a broad shoulder at ∼800−950 cm^{-1} on the absorbance peak for the Al−F stretching vibrations that may be partially assigned to the libration of HF molecules on the AlF_3 surface.[26,39] Absorbance features for the H−F stretching vibration in isolated and hydrogen-bonded HF on the AlF_3 surface were also observed at higher frequencies of

DOI: 10.1021/acs.jpcc.5b07236
J. Phys. Chem. C 2015, 119, 25385−25393

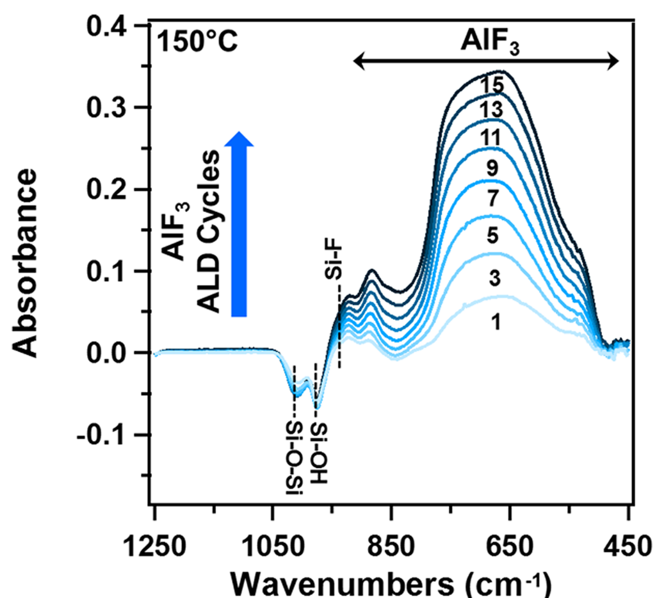

Figure 8. Absolute infrared absorbance showing the growth of Al−F stretching vibrations in AlF_3 versus number of AlF_3 ALD cycles at 150 °C. These FTIR spectra were referenced to the initial SiO_2 nanoparticles.

~3000−3675 cm^{-1} during AlF_3 ALD.[26] There also is absorbance at 930 cm^{-1} that may be assigned to the formation of Si−F bonds on the SiO_2 nanoparticles during AlF_3 growth.[40] The absorbance losses at 975 and 1010 cm^{-1} are attributed to the loss of Si−OH and Si−O−Si species on the initial SiO_2 substrate, respectively.[41] There is no evidence for any pyridine features in the FTIR spectrum. This observation is consistent with no measurable pyridine in the gas phase above HF-pyridine.[24,26]

Figure 9 shows the FTIR spectra after 4, 6, 8, 10, and 12 AlF_3 ALE cycles at 250 °C. These FTIR spectra were recorded after

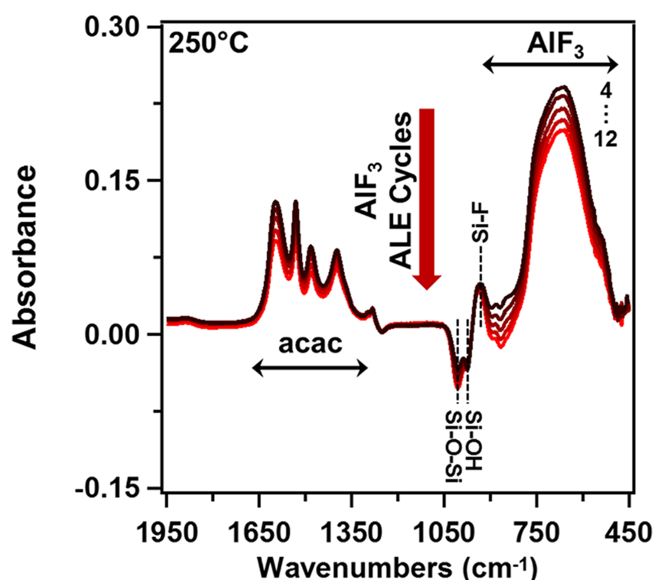

Figure 9. Absolute infrared absorbance showing the loss of Al−F stretching vibrations in AlF_3 versus number of AlF_3 ALE cycles at 250 °C. The $Sn(acac)_2$ exposures also lead to the appearance of acac surface species. These FTIR spectra were referenced to the initial SiO_2 nanoparticles.

$Sn(acac)_2$ exposures and are also referenced to the FTIR spectrum for the SiO_2 nanoparticles. Decreasing absorbance for the Al−F stretching vibrations between 500 and 900 cm^{-1} versus ALE cycles is consistent with AlF_3 etching. Infrared absorbance for the $Sn(acac)_2$ adsorption products is also observed between 1250 and 1650 cm^{-1}. These vibrational features are consistent with acac-containing species such as $AlF_2(acac)$*, $Sn(acac)_2$*, or SnF(acac)* adsorbed on the AlF_3 substrate.[42,43]

Figure 10 displays the FTIR spectra after consecutive $Sn(acac)_2$ and HF exposures at 250 °C. These FTIR spectra

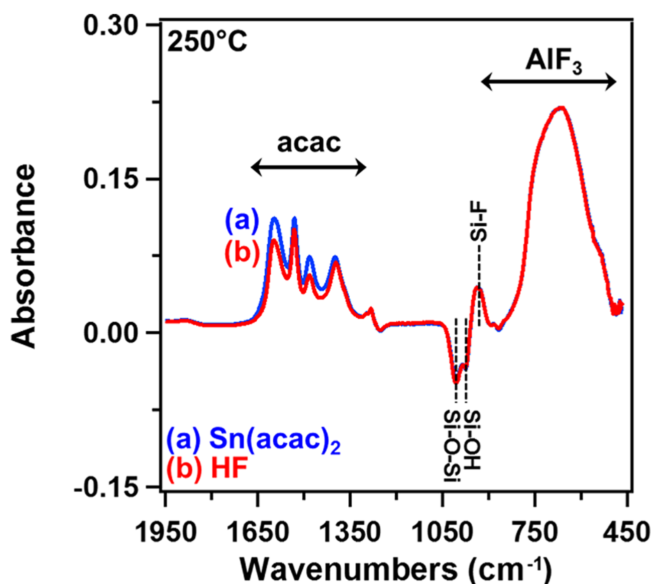

Figure 10. FTIR spectra for consecutive $Sn(acac)_2$ and HF exposures at 250 °C referenced to the FTIR spectrum for the SiO_2 nanoparticles. (a) Spectrum after $Sn(acac)_2$ exposure. (b) Spectrum after HF exposure.

were referenced to the FTIR spectrum for the SiO_2 nanoparticles. Over the frequency region from 1250 to 1650 cm^{-1}, the absorbance change indicates that the HF exposure removes only ~20% of the total acac-containing species on the surface at 250 °C. These results demonstrate that the HF exposure is only affecting a small fraction of the total acac-containing species. A large number of acac-containing species reside on the AlF_3 surface without changing as a result of the $Sn(acac)_2$ and HF exposures.

Figure 11 shows the FTIR difference spectra for the same consecutive $Sn(acac)_2$ and HF exposures at 250 °C that are displayed in Figure 10. These difference spectra are defined by referencing to the spectra after the previous reactant exposure. Figure 11a shows the difference spectrum after the $Sn(acac)_2$ exposure that has been referenced to the spectrum after the previous HF exposure. Figure 11a shows absorbance gains for the vibrational features between 1250 and 1650 cm^{-1} and absorbance loss for the vibrational feature between 500 and 900 cm^{-1}. The absorbance loss between 500 and 900 cm^{-1} is consistent with the removal of Al−F stretching vibrations as $Sn(acac)_2$ reacts with the AlF_3 surface layer and removes fluorine and aluminum by the formation of volatile SnF(acac), $AlF_2(acac)$, or $Al(acac)_2$ reaction products. The absorbance gain between 1250 and 1650 cm^{-1} is consistent with the addition of acac-containing reaction products on the AlF_3 substrate.

DOI: 10.1021/acs.jpcc.5b07236
J. Phys. Chem. C 2015, 119, 25385−25393

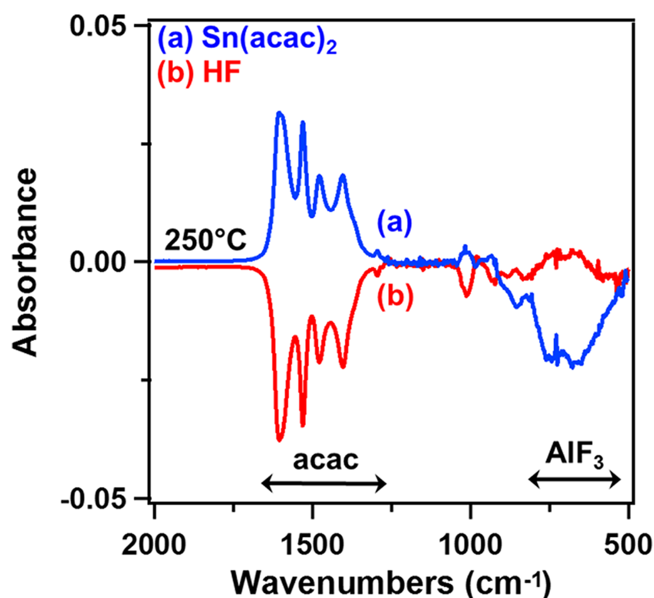

Figure 11. FTIR difference spectra for the same consecutive $Sn(acac)_2$ and HF exposures at 250 °C shown in Figure 10. (a) Difference spectrum after $Sn(acac)_2$ exposure defined by referencing to the spectrum after the previous HF exposure. (b) Difference spectrum after the HF exposure defined by referencing to the spectrum after the previous $Sn(acac)_2$ exposure.

Figure 11b displays the difference spectrum after the HF exposure that has been referenced to the spectrum after the previous $Sn(acac)_2$ exposure. The absorbance features for acac-containing species that were added between 1250 and 1650 cm^{-1} as a result of the $Sn(acac)_2$ exposure are taken away by the subsequent HF exposure. There is also a small increase in absorbance between 500 and 900 cm^{-1}. This small absorbance increase is in the region corresponding to the Al−F stretching vibrations.[35−38] This absorbance increase may result from the HF exposure converting some $AlF_2(acac)^*$ surface species back to AlF_3^* species by the reaction $AlF_2(acac)^* + HF \rightarrow AlF_3^* +$ acacH.

Figures 10 and 11 indicate that HF is necessary for AlF_3 ALE because the HF exposures remove or convert some acac-containing surface species. The removal of these acac-containing species allows $Sn(acac)_2$ to etch the underlying AlF_3 substrate. These FTIR results also suggest that $Sn(acac)_2$ cannot spontaneously etch AlF_3 because the etching is self-limited by the buildup of acac-containing species on the AlF_3 surface. These acac-containing surface species, such as $AlF_2(acac)^*$, $AlF(acac)_2^*$, or $SnF(acac)^*$, may block the AlF_3 etching.

C. AlF_3 ALE Reaction Mechanisms. The results from the in situ QCM and FTIR measurements can be used to propose a reaction mechanism for AlF_3 ALE. The reaction mechanism depends on the identity of the surface intermediate. The most likely surface intermediates are $AlF_2(acac)^*$ and $SnF(acac)^*$. The QCM analysis cannot easily discriminate between the $AlF_2(acac)^*$ and $SnF(acac)^*$ surface intermediates. Although $SnF(acac)^*$ is heavier than $AlF_2(acac)^*$, there could be more $AlF_2(acac)^*$ on the surface to yield the observed mass changes. In contrast, the FTIR analysis provides support for an $AlF_2(acac)^*$ surface intermediate based on the gain in absorbance for the Al−F stretching vibration during HF exposures observed in Figure 11b.

Figure 12 shows a schematic of the AlF_3 ALE reaction mechanism based on an $AlF_2(acac)^*$ surface intermediate. This

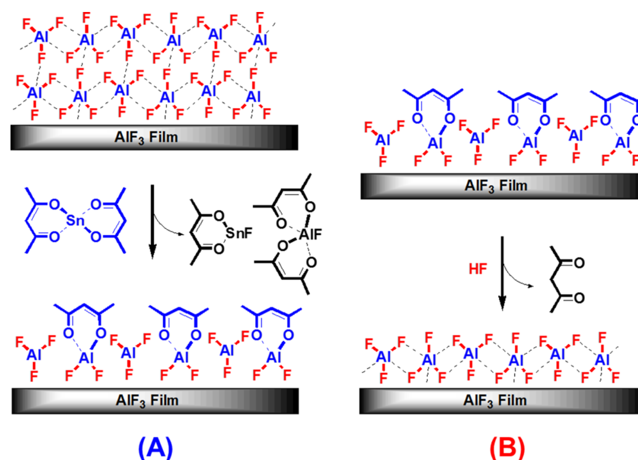

Figure 12. Schematic of proposed reaction mechanism for AlF_3 ALE based on $AlF_2(acac)^*$ intermediate showing (A) $Sn(acac)_2$ reaction and (B) HF reaction.

schematic shows only the species that change during the reactions. The dashed lines in the AlF_3 adlayer are intended to represent the distorted octahedral structure in the AlF_3 solid. In reaction (A), $Sn(acac)_2$ is exposed to the AlF_3 surface and forms SnF(acac) and $AlF(acac)_2$ as volatile reaction products. Reaction (A) also leads to $AlF_2(acac)^*$ intermediates on the AlF_3 surface. In reaction (B), HF converts the $AlF_2(acac)^*$ intermediates into AlF_3^* surface species and volatile acacH.

This overall reaction can be expressed as

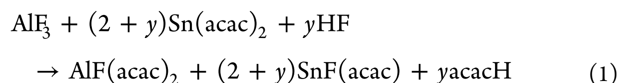

$$AlF_3 + (2 + y)Sn(acac)_2 + yHF \rightarrow AlF(acac)_2 + (2 + y)SnF(acac) + y\,acacH \quad (1)$$

This overall reaction can be divided into the $Sn(acac)_2$ and HF reactions:

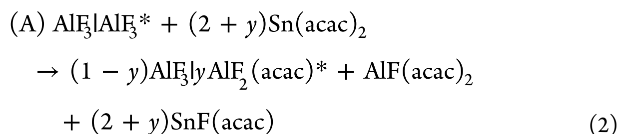

$$(A)\ AlF_3|AlF_3^* + (2 + y)Sn(acac)_2 \rightarrow (1 - y)AlF_3|yAlF_2(acac)^* + AlF(acac)_2 + (2 + y)SnF(acac) \quad (2)$$

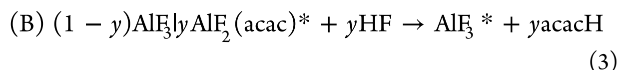

$$(B)\ (1 - y)AlF_3|yAlF_2(acac)^* + yHF \rightarrow AlF_3^* + y\,acacH \quad (3)$$

$AlF_2(acac)^*$ is the key reaction intermediate. In reaction (B), HF reacts with $AlF_2(acac)^*$ to produce AlF_3^* surface species and volatile acacH.

The AlF_3^* species shown in eq 2 is the amount of AlF_3 that is etched during one cycle of AlF_3 ALE. y quantifies the $AlF_2(acac)^*$ intermediate species that are produced by the $Sn(acac)_2$ exposure relative to the amount of AlF_3 that is etched in one AlF_3 ALE cycle. The parameter y in eqs 2 and 3 is determined by the ΔM_{Sn}, ΔM_{HF}, and MCPC values determined by the QCM analysis.

y can be obtained from the ΔM_{Sn}/MCPC ratio using the equation

$$y = (84.0 - 84.0(\Delta M_{Sn}/MCPC))/(164.1 - 84.0) \quad (4)$$

where 84.0 and 164.1 are the molecular weights for AlF_3 and $AlF_2(acac)^*$, respectively. The temperature dependence of the y

DOI: 10.1021/acs.jpcc.5b07236
J. Phys. Chem. C 2015, 119, 25385−25393

values is y = 4.0, 1.2, and 0.40 at 150, 200, and 250 °C, respectively. These y values are included in Table 1.

The product y(MCPC) is a measure of the absolute AlF_2(acac)* intermediate surface coverage that is formed by the $Sn(acac)_2$ exposure. The y(MCPC) values are summarized in Table 1. The y(MCPC) values are fairly constant at the various temperatures. This trend indicates that the AlF_2(acac)* intermediate coverage is nearly equal at the different temperatures.

The absolute AlF_2(acac)* coverage after the $Sn(acac)_2$ exposures can be obtained from the amount of AlF_3 that is etched in one AlF_3 ALE cycle. The MCPC of −6.1 ng/cm^2 at 200 °C represents a coverage of 4.4 × 10^{13} (AlF_3 units)/cm^2. This coverage of (AlF_3 units) multiplied by the y value of 1.20 at 200 °C yields an absolute AlF_2(acac)* coverage of 5.28 × 10^{13} AlF_2(acac)*/cm^2. The MCPC and y values at other temperatures also yield similar absolute AlF_2(acac)* coverages that vary from 5.24 to 5.76 × 10^{13} AlF_2(acac)*/cm^2.

The nearly constant absolute AlF_2(acac)* coverage of ~5.5 × 10^{13} AlF_2(acac)*cm^2 can be compared with the number of (AlF_3 units) on the AlF_3 surface. The normalized coverage of AlF_2(acac)* relative to (AlF_3 units) on the surface is (~5.5 × 10^{13} AlF_2(acac)*/cm^2)/(4.76 × 10^{14} (AlF_3 unit)/cm^2) = ~0.116 AlF_2(acac)*/(AlF_3 unit). This normalized coverage is ~11.6% of an (AlF_3 unit) monolayer.

The proposed reactions for AlF_3 ALE are also very similar to the reactions suggested earlier for Al_2O_3 and HfO_2 ALE.[22−24] The main difference is the lack of a fluorination step during AlF_3 ALE. However, the HF exposure is still required to remove acac-containing surface species that limit etching during the $Sn(acac)_2$ exposure. Al_2O_3 ALE displays etching rates that increase at higher temperatures.[22,23] Based on the previous Al_2O_3 ALE studies,[22] these temperature-dependent etching rates are thought to be correlated inversely with the total coverage of acac-containing species on the substrate after the HF or $Sn(acac)_2$ exposures. The etching rates for AlF_3 ALE are also comparable with the etching rates for Al_2O_3 and HfO_2 ALE.

IV. CONCLUSIONS

The thermal ALE of a metal fluoride was demonstrated for the first time using sequential thermal reactions with $Sn(acac)_2$ and HF as the reactants. In situ quartz crystal microbalance (QCM) and Fourier transform infrared (FTIR) measurements were employed to examine AlF_3 ALE at temperatures from 150 to 250 °C. The QCM measurements showed that AlF_3 was etched linearly versus the number of sequential $Sn(acac)_2$ and HF reactant exposures. The FTIR spectroscopic measurements monitored AlF_3 etching by observing the loss of absorbance of Al−F stretching vibrations in the AlF_3 film. The QCM studies verified that the sequential $Sn(acac)_2$ and HF reactions were self-limiting versus reactant exposure. The QCM analysis also showed that the mass change per cycle (MCPC) increased with temperature from −2.0 ng/(cm^2 cycle) at 150 °C to −18.2 ng/(cm^2 cycle) at 250 °C. These MCPC values are equivalent to etch rates varying from 0.069 Å/cycle at 150 °C to 0.63 Å/cycle at 250 °C.

The results from the QCM and FTIR studies suggest a likely reaction mechanism for AlF_3 ALE. The $Sn(acac)_2$ reactant accepts fluorine from AlF_3 to form volatile SnF(acac) reaction products and also donates acac to AlF_3 to produce volatile reaction products such as $AlF(acac)_2$. In addition, the $Sn(acac)_2$ exposure also produces acac-containing species on the AlF_3 surface that restrict the $Sn(acac)_2$ etching reaction. Without these acac-containing species, the etching of AlF_3 by $Sn(acac)_2$ would not be expected to be self-limiting. The HF reactant then removes some of the acac-containing species and allows more etching to proceed during the next $Sn(acac)_2$ exposure. A reaction mechanism for AlF_3 ALE was suggested based on an AlF_2(acac)* intermediate surface species. Similar reaction mechanisms should be applicable to the ALE of other metal fluorides using $Sn(acac)_2$ and HF. This study also provides insight into the reaction mechanism of Al_2O_3 ALE because Al_2O_3 ALE involves an AlF_3 reaction intermediate.

■ AUTHOR INFORMATION

Notes

The authors declare no competing financial interest.

■ ACKNOWLEDGMENTS

This research was funded by the National Science Foundation (CHE-1306131). Additional personnel support for Y.L. was provided by the Department of Energy through the DOE-BATT program.

■ REFERENCES

(1) Agarwal, A.; Kushner, M. J. Plasma Atomic Layer Etching Using Conventional Plasma Equipment. *J. Vac. Sci. Technol., A* **2009**, *27*, 37−50.

(2) Carver, C. T.; Plombon, J. J.; Romero, P. E.; Suri, S.; Tronic, T. A.; Turkot, R. B. Atomic Layer Etching: An Industry Perspective. *ECS J. Solid State Sci. Technol.* **2015**, *4*, N5005−N5009.

(3) Oehrlein, G. S.; Metzler, D.; Li, C. Atomic Layer Etching at the Tipping Point: An Overview. *ECS J. Solid State Sci. Technol.* **2015**, *4*, N5041−N5053.

(4) Faraz, T.; Roozeboom, F.; Knoops, H. C. M.; Kessels, W. M. M. Atomic Layer Etching: What Can We Learn from Atomic Layer Deposition? *ECS J. Solid State Sci. Technol.* **2015**, *4*, N5023−N5032.

(5) George, S. M. Atomic Layer Deposition: An Overview. *Chem. Rev.* **2010**, *110*, 111−131.

(6) Athavale, S. D.; Economou, D. J. Realization of Atomic Layer Etching of Silicon. *J. Vac. Sci. Technol., B: Microelectron. Process. Phenom.* **1996**, *14*, 3702−3705.

(7) Park, S. D.; Lee, D. H.; Yeom, G. Y. Atomic Layer Etching of Si(100) and Si(111) Using Cl_2 and Ar Neutral Beam. *Electrochem. Solid-State Lett.* **2005**, *8*, C106−C109.

(8) Sakaue, H.; Iseda, S.; Asami, K.; Yamamoto, J.; Hirose, M.; Horiike, Y. Atomic Layer Controlled Digital Etching of Silicon. *Jpn. J. Appl. Phys. 1* **1990**, *29*, 2648−2652.

(9) Yamamoto, J.; Kawasaki, T.; Sakaue, H.; Shingubara, S.; Horiike, Y. Digital Etching Study and Fabrication of Fine Si Lines and Dots. *Thin Solid Films* **1993**, *225*, 124−129.

(10) Sugiyama, T.; Matsuura, T.; Murota, J. Atomic-Layer Etching of Ge Using an Ultraclean ECR Plasma. *Appl. Surf. Sci.* **1997**, *112*, 187−190.

(11) Lim, W. S.; Park, S. D.; Park, B. J.; Yeom, G. Y. Atomic Layer Etching of (100)/(111) GaAs with Chlorine and Low Angle Forward Reflected Ne Neutral Beam. *Surf. Coat. Technol.* **2008**, *202*, 5701−5704.

(12) Meguro, T.; Hamagaki, M.; Modaressi, S.; Hara, T.; Aoyagi, Y.; Ishii, M.; Yamamoto, Y. Digital Etching of GaAsNew Approach of Dry Etching to Atomic Ordered Processing. *Appl. Phys. Lett.* **1990**, *56*, 1552−1554.

(13) Meguro, T.; Ishii, M.; Sugano, T.; Gamo, K.; Aoyagi, Y. Control of the Etching Reaction of Digital Etching Using Tunable UV Laser Irradiation. *Appl. Surf. Sci.* **1994**, *82−83*, 193−199.

(14) Park, S. D.; Oh, C. K.; Bae, J. W.; Yeom, G. Y.; Kim, T. W.; Song, J. I.; Jang, J. H. Atomic Layer Etching of InP Using a Low Angle

DOI: 10.1021/acs.jpcc.5b07236
J. Phys. Chem. C 2015, 119, 25385−25393

Forward Reflected Ne Neutral Beam. *Appl. Phys. Lett.* **2006**, *89*, 043109.
(15) Park, J. B.; Lim, W. S.; Park, S. D.; Park, Y. J.; Yeom, G. Y. Etch Characteristics of TiO_2 Etched by Using an Atomic Layer Etching Technique with BCl_3 Gas and an Ar Neutral Beam. *J. Korean Phys. Soc.* **2009**, *54*, 976–980.
(16) Metzler, D.; Bruce, R. L.; Engelmann, S.; Joseph, E. A.; Oehrlein, G. S. Fluorocarbon Assisted Atomic Layer Etching of SiO_2 using Cyclic Ar/C_4F_8 Plasma. *J. Vac. Sci. Technol., A* **2014**, *32*, 020603.
(17) Min, K. S.; Kang, S. H.; Kim, J. K.; Jhon, Y. I.; Jhon, M. S.; Yeom, G. Y. Atomic Layer Etching of Al_2O_3 Using BCl_3/Ar for the Interface Passivation Layer of III–V MOS Devices. *Microelectron. Eng.* **2013**, *110*, 457–460.
(18) Park, J. B.; Lim, W. S.; Park, B. J.; Park, I. H.; Kim, Y. W.; Yeom, G. Y. Atomic Layer Etching of Ultra-Thin HfO_2 Film for Gate Oxide in MOSFET Devices. *J. Phys. D: Appl. Phys.* **2009**, *42*, 055202.
(19) Kim, Y. Y.; Lim, W. S.; Park, J. B.; Yeom, G. Y. Layer by Layer Etching of the Highly Oriented Pyrolythic Graphite by Using Atomic Layer Etching. *J. Electrochem. Soc.* **2011**, *158*, D710–D714.
(20) Lim, W. S.; Kim, Y. Y.; Kim, H.; Jang, S.; Kwon, N.; Park, B. J.; Ahn, J.-H.; Chung, I.; Hong, B. H.; Yeom, G. Y. Atomic Layer Etching of Graphene for Full Graphene Device Fabrication. *Carbon* **2012**, *50*, 429–435.
(21) Vogli, E.; Metzler, D.; Oehrlein, G. S. Feasibility of Atomic Layer Etching of Polymer Material Based on Sequential O_2 Exposure and Ar Low-Pressure Plasma-Etching. *Appl. Phys. Lett.* **2013**, *102*, 253105.
(22) Lee, Y.; DuMont, J. W.; George, S. M. Mechanism of Thermal Al_2O_3 Atomic Layer Etching Using Sequential Thermal Reactions with $Sn(acac)_2$ and HF. *Chem. Mater.* **2015**, *27*, 3648–3657.
(23) Lee, Y.; George, S. M. Atomic Layer Etching of Al_2O_3 Using Sequential, Self-Limiting Thermal Reactions with $Sn(acac)_2$ and HF. *ACS Nano* **2015**, *9*, 2061–2070.
(24) Lee, Y.; DuMont, J. W.; George, S. M. Atomic Layer Etching of HfO_2 Using Sequential, Self-Limiting Thermal Reactions with $Sn(acac)_2$ and HF. *ECS J. Solid State Sci. Technol.* **2015**, *4*, N5013–N5022.
(25) Spessard, G. O.; Miessler, G. L. *Organometallic Chemistry*, 3rd. ed.; Oxford University Press: New York, 2016.
(26) Lee, Y.; DuMont, J. W.; Cavanagh, A. S.; George, S. M. Atomic Layer Deposition of AlF_3 Using Trimethylaluminum and Hydrogen Fluoride. *J. Phys. Chem. C* **2015**, *119*, 14185–14194.
(27) Elam, J. W.; Groner, M. D.; George, S. M. Viscous Flow Reactor with Quartz Crystal Microbalance for Thin Film Growth by Atomic Layer Deposition. *Rev. Sci. Instrum.* **2002**, *73*, 2981–2987.
(28) DuMont, J. W.; George, S. M. Pyrolysis of Alucone Molecular Layer Deposition Films Studied Using In Situ Transmission Fourier Transform Infrared Spectroscopy. *J. Phys. Chem. C* **2015**, *119*, 14603–14612.
(29) Ballinger, T. H.; Wong, J. C. S.; Yates, J. T. Transmission Infrared-Spectroscopy of High Area Solid-Surfaces—A Useful Method for Sample Preparation. *Langmuir* **1992**, *8*, 1676–1678.
(30) Ferguson, J. D.; Weimer, A. W.; George, S. M. Atomic Layer Deposition of Ultrathin and Conformal Al_2O_3 Films on BN Particles. *Thin Solid Films* **2000**, *371*, 95–104.
(31) Nakanishi, K.; Toyama, O. Vapor-Pressure of Acetylacetone Below Normal Boiling-Point. *Bull. Chem. Soc. Jpn.* **1972**, *45*, 3210–3211.
(32) Bos, K. D.; Budding, H. A.; Bulten, E. J.; Noltes, J. G. Tin(II) Bis(1,3-diketonates) and TiN(II) 1,3-Diketonate Chlorides. *Inorg. Nucl. Chem. Lett.* **1973**, *9*, 961–963.
(33) Berg, E. W.; Truemper, J. T. Vapor Pressure-Temperature Data for Various Metal Beta-Diketone Chelates. *Anal. Chim. Acta* **1965**, *32*, 245–252.
(34) Fahlman, B. D.; Barron, A. R. Substituent Effects on the Volatility of Metal Beta-Diketonates. *Adv. Mater. Opt. Electron.* **2000**, *10*, 223–232.
(35) Gross, U.; Rüdiger, S.; Kemnitz, E.; Brzezinka, K.-W.; Mukhopadhyay, S.; Bailey, C.; Wander, A.; Harrison, N. Vibrational Analysis Study of Aluminum Trifluoride Phases. *J. Phys. Chem. A* **2007**, *111*, 5813–5819.
(36) Heitmann, W. Vacuum Evaporated Films of Aluminum Fluoride. *Thin Solid Films* **1970**, *5*, 61–67.
(37) König, R.; Scholz, G.; Scheurell, K.; Heidemann, D.; Buchem, I.; Unger, W. E. S.; Kemnitz, E. Spectroscopic Characterization of Crystalline AlF_3 Phases. *J. Fluorine Chem.* **2010**, *131*, 91–97.
(38) Utkin, A. N.; Girichev, G. V.; Giricheva, N. I.; Khaustov, S. V. Structure and Vibrational Frequencies of Aluminum Trifluoride and Gallium Trifluoride. *J. Struct. Chem.* **1986**, *27*, 212–215.
(39) Ayotte, P.; Hebert, M.; Marchand, P. Why is Hydrofluoric Acid a Weak Acid? *J. Chem. Phys.* **2005**, *123*, 184501.
(40) Wang, P. F.; Ding, S. J.; Zhang, W.; Zhang, J. Y.; Wang, J. T.; Wei, W. L. FTIR Characterization of Fluorine Doped Silicon Dioxide Thin Films Deposited by Plasma Enhanced Chemical Vapor Deposition. *Chin. Phys. Lett.* **2000**, *17*, 912–914.
(41) Kinney, J. B.; Staley, R. H. Reactions of Titanium Tetrachloride and Trimethylaluminum at Silica Surfaces Studied by Using Infrared Photo-Acoustic Spectroscopy. *J. Phys. Chem.* **1983**, *87*, 3735–3740.
(42) Nakamoto, K.; Martell, A. E.; McCarthy, P. J. Infrared Spectra of Metal Chelate Compounds. 3. Infrared Spectra of Acetylacetonates of Divalent Metals. *J. Am. Chem. Soc.* **1961**, *83*, 1272–1276.
(43) Tayyari, S. F.; Milani-nejad, F. Vibrational Assignment of Acetylacetone. *Spectrochim. Acta, Part A* **2000**, *56*, 2679–2691.

DOI: 10.1021/acs.jpcc.5b07236
J. Phys. Chem. C 2015, 119, 25385–25393